UC Berkeley
UC Berkeley Previously Published Works

Title

Sequestration-based bistability enables tuning of the switching boundaries and design of a latch

Permalink

https://escholarship.org/uc/item/2sc1h18p

Journal

Molecular Systems Biology, 8(1)

ISSN

1744-4292

Authors

Chen, David
Arkin, Adam P

Publication Date

2012

DOI

10.1038/msb.2012.52

Peer reviewed

REPORT

Sequestration-based bistability enables tuning of the switching boundaries and design of a latch

David Chen[1,2] and Adam P Arkin[2,3,4,*]

[1] The UC Berkeley-UCSF Graduate Program in Bioengineering, Berkeley, CA, USA, [2] Department of Bioengineering, University of California, Berkeley, CA, USA, [3] Physical Biosciences Division, Lawrence Berkeley National Lab, Berkeley, CA, USA and [4] QB3: California Institute for Quantitative Biological Research, University of California, Berkeley, CA, USA
* Corresponding author. Department of Bioengineering, University of California, Berkeley, 512C Energy Biosciences Building, Mailstop Stanley 922, Berkeley, CA 94720, USA. Tel.: +1 510 206 1389; Fax: +1 510 486 6059; E-mail: aparkin@lbl.gov

Natural biological systems have evolved a diverse array of switches to realize their strategies for environmental response and development. Emerging applications of synthetic biology have begun to exploit such switches to achieve increasingly sophisticated designed behaviors. However, not all switch architectures allow facile design of the switching and memory properties. Furthermore, not all designs are built from components for which large families of variants exist, a requirement for building many orthogonal switch variants. Therefore, there is a critical need from genetic engineers for scalable strategies that yield custom bistable switches. Here, we use a sigma factor and its cognate anti-sigma factor to experimentally verify that ultrasensitivity from sequestration combined with positive feedback is sufficient to build a bistable switch. We show that sequestration allows us to predictably tune the switching boundaries, and we can easily tune our switch to function as a set–reset latch that can be toggled between two states by a pulse of inducer input.
Molecular Systems Biology 8:620; published online 23 October 2012; doi:10.1038/msb.2012.52
Subject Categories: synthetic biology
Keywords: bistability; genetic circuits; nonlinear dynamics; sequestration; synthetic biology

Introduction

Bistable switches represent the canonical solution for building memory units that also generate noise-tolerant sigmoidal responses to inputs (Ferrell, 2002; Burrill and Silver, 2010). Bistability in a dynamical system, such as a genetic switch, requires positive feedback (either directly or indirectly, as shown in Figure 1A) and any source of ultrasensitivity that generates a sigmoidal response (Ferrell, 1996; Angeli *et al*, 2004; Ray *et al*, 2011). While Figure 1B shows a number of commonly proposed sources of ultrasensitivity, currently all synthetic bistable systems rely on cooperativity (Gardner *et al*, 2000; Becskei *et al*, 2001; Atkinson *et al*, 2003; Kramer and Fussenegger, 2005; Ajo-Franklin *et al*, 2007), with possible exceptions considered in the Discussion section. In addition, all known natural bistable systems also utilize cooperativity, although often in combination with other sources of ultrasensitivity (Ozbudak *et al*, 2004; Acar *et al*, 2005; Trunnell *et al*, 2011).

Despite the prevalence of cooperativity, recent work has shown sequestration's importance in natural systems (Kim and Ferrell, 2007; Buchler and Louis, 2008), and sequestration-based ultrasensitivity has been demonstrated synthetically in eukaryotic systems (Bashor *et al*, 2008; Buchler and Cross, 2009; Lu *et al*, 2011; Lee and Maheshri, 2012). Curiously, no one has yet demonstrated *in vivo* that sequestration with positive feedback is

sufficient to build a bistable switch, but the design shown in Figure 1C should have beneficial design properties. As the minimal requirements are an activator to build the positive feedback loop and a tight-binding anti-activator, the design is generalizable to many potential parts. In addition, Figure 1D illustrates that the response curve from sequestration can be predictably adjusted by varying the expression level of the anti-activator, and we demonstrate how this property can be utilized to predictably tune the switching boundaries.

Results

We chose to demonstrate our sequestration-based switch in *Escherichia coli* (*Ec*), using the *sigW* sigma factor and its cognate anti-sigma factor (*rsiW*) from *Bacillus subtilis* as the activator and anti-activator (see Materials and methods for cloning details and Figure 2A for schematic). To build the positive feedback loop, we placed the sigma factor under control of a SigW-dependent promoter. Expression of the anti-sigma factor was controlled by an arabinose-inducible promoter. Finally, system output was monitored by placing YFP expression under control of the SigW-responsive promoter.

We call the cells ON when the positive feedback loop is active and YFP is expressed, and cells without YFP expression
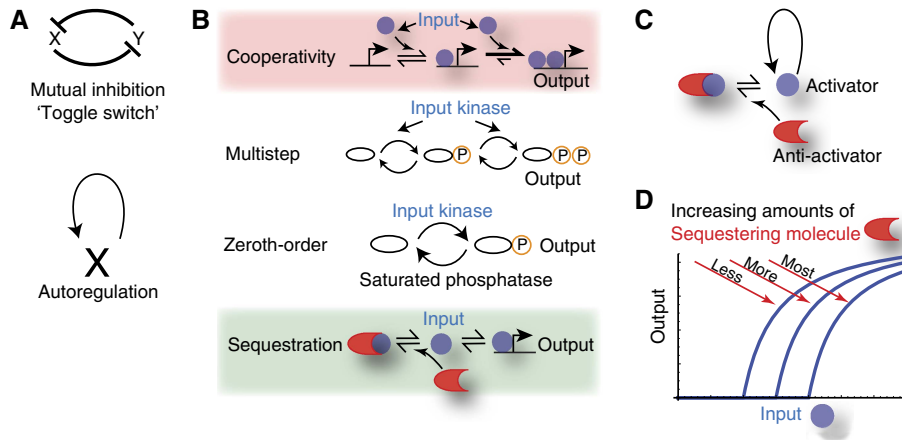
Figure 1 Required elements for building a bistable switch. (**A**) Positive feedback can be indirect from mutual inhibition or direct from autoregulation. (**B**) Four commonly proposed sources of ultrasensitivity. Cooperativity (shaded in red) is the most prevalent source in known bistable systems, but we demonstrate that sequestration (shaded in green) can be used to build a bistable switch with better design features. (**C**) The sequestration-based switch requires an activator that forms a positive feedback loop and an anti-activator that sequesters activator molecules. (**D**) The response curve from sequestration can be shifted to the left and right by changing the expression level of the sequestering molecule.
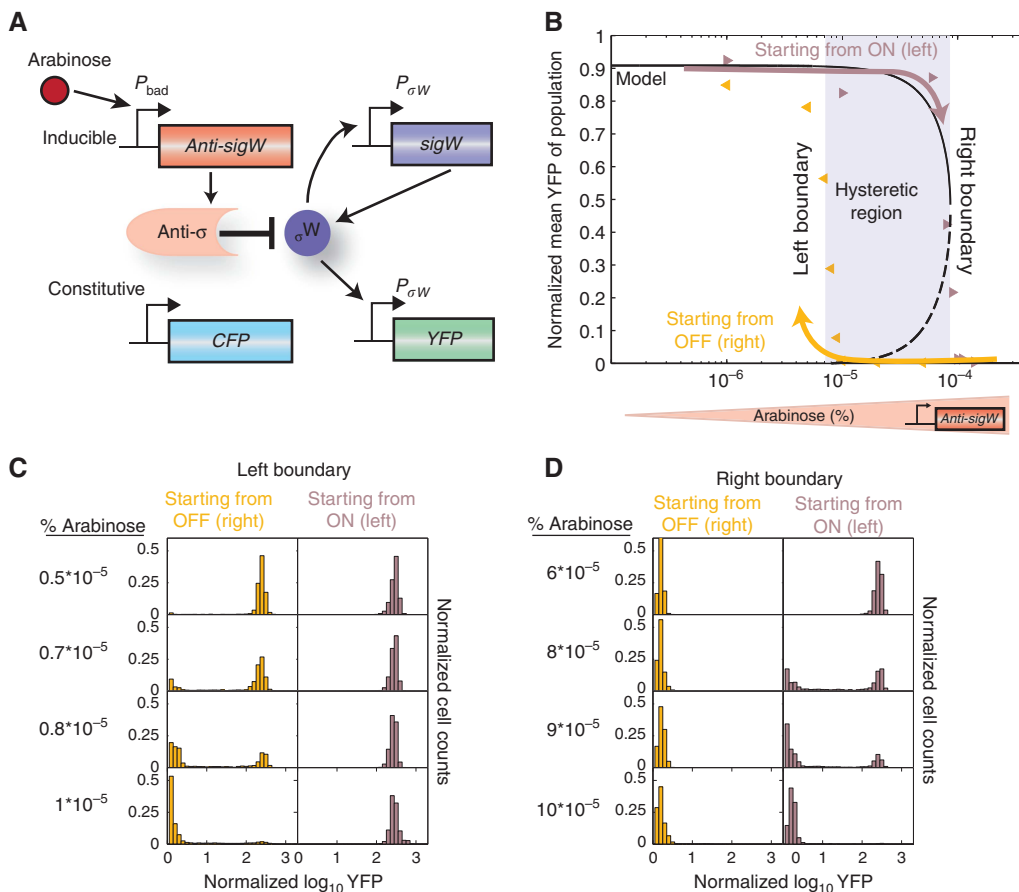

Figure 2 Sequestration with positive feedback is sufficient for bistability *in vivo*. (**A**) Schematic of construct implemented in APA4309 *E. coli* cells using a sigma factor and anti-sigma factor from *B. subtilis*. Cerulean (CFP) is expressed constitutively in all cells to detect dead cells and for normalization. (**B**) Cells previously grown in full or no arabinose induction were inoculated into intermediate concentrations and grown for 12 h. The right arrowheads in maroon color show the mean fluorescence of cells previously grown in no arabinose (initially ON). The left arrowheads in orange color show the mean fluorescence of cells previously grown in full arabinose induction (initially OFF). The y axis is the mean YFP of the population after normalizing each cell by its CFP fluorescence. The shaded area shows the hysteretic region where the system retains a memory of its previous state. (**C, D**) Histograms at indicated arabinose concentrations show bimodal distributions at the switching boundaries. The x axis shows $\log_{10}$ YFP fluorescence normalized by each cell's CFP fluorescence and y axis shows the normalized cell count. At least 1000 cells were imaged at each induction point. Source data is available for this figure in the Supplementary Information.

are considered OFF. The defining feature of bistability is a hysteretic region where the steady-state response of the system depends on the previous state. Supplementary Figure 1 presents the nullclines for this system and illustrates why we expect to observe hysteresis as anti-sigma factor expression is varied. To experimentally locate this region, we grew cells in the absence of arabinose and at full induction (0.1%) overnight and then stored both sets of aliquots at $-80°C$. The cells from the aliquots were then inoculated into intermediate arabinose concentrations and allowed to grow for 24 doublings before being imaged by fluorescence microscopy. Figure 2B shows the memory region where the system responds differently depending on whether it was previously ON or OFF. Cells that were previously in full arabinose induction remain OFF in the memory region and then begin to turn ON at 10^{-5}% arabinose (orange arrowheads facing left). Cells that were previously grown in the absence of arabinose are fully ON in the memory region and begin to switch OFF at $8*10^{-4}$% arabinose (maroon-colored arrowheads facing right). Constitutive CFP expression was used to normalize the YFP expression and eliminate dead cells from the analysis. Figure 2B also shows our model overlaid with the experimentally determined points (see Supplementary information for modeling details). Figure 2C and D show that the distribution of cells in the ON and OFF states shifts at the switching boundaries. We found that ON cells grew ~ 4.5% slower than OFF cells (Supplementary Table 1). Using a model recently published for stochastic switching between phenotypes with different growth rates (Nevozhay et al, 2012), we found that ON cells switched OFF in the memory region at a rate of 0.0165 ± 0.014 per hour while OFF cells switched ON at a much slower rate of $6.1*10^{-4} \pm 7*10^{-5}$ per hour (Supplementary Figure 2). We also verified that the sigma factor does not exhibit intrinsic cooperativity (Supplementary Figure 3) and that the state of the switch does not affect expression from a constitutive Sigma 70 promoter (Supplementary Figure 4). To demonstrate that our design is not specific to SigW, we also demonstrated hysteresis in a bistable system based on SigE and its cognate anti-sigma factor ChrR from *Rhodobacter sphaeroides* (Supplementary Figure 5).

To tune the switching boundaries of our sequestration-based switch, we added another transcriptional unit with the sigma factor under control of a promoter inducible with anhydrotetracycline (aTc) (schematic shown in Figure 3A). In this system, the two induced proteins compete with each other. In the limit of high expression of anti-sigma factor and no sigma factor induction, all the cells are turned OFF. In the other limit where the sigma factor is strongly induced and no anti-sigma factor is present, all the cells are forced ON. In between the two extremes, we expect a bistable region whose boundaries vary with the total concentrations of the proteins. The numerically computed bifurcation diagram for this system is plotted in Figure 3B. We predict that cells at higher levels of sigma factor (aTc) induction require higher levels of anti-sigma factor (arabinose) induction to cross the boundaries. We experimentally verified this relationship by preparing aliquots of master cultures that were forced to be OFF or ON. Initially, OFF cells were grown at the inducer concentrations indicated in Figure 3B with left arrowheads, and we found that increasing

aTc concentration results in switching ON at higher arabinose concentrations, shown in Figure 3C. Similarly, initially ON cells were grown at the concentrations indicated with right arrowheads, and we found that increasing aTc concentration requires higher levels of arabinose to switch OFF, shown in Figure 3D.

From the bifurcation diagram, we also predicted that we could design our switch to function as a set–reset latch. The latch is a true memory element rather than a hysteretic switch. It holds the state of the last input: set or reset. Figure 3E illustrates that the two inputs to the latch are arabinose and aTc, and Figure 3F shows the logic table the set–reset latch implements. To demonstrate the latch with APA4310 cells, we sequentially performed the steps illustrated in the bifurcation diagram of Figure 3G. We first initialized the latch into the reset state by forcing the cells OFF with full induction of anti-sigma factor (step 1 of Figure 3G and response shown in Figure 3H). We then inoculated the cells with both inputs set low, so the cells are in the memory state and remain OFF (step 2). While maintaining the same concentration of arabinose, we pulsed the cells into the ON state by growing them in aTc and observed that upon inoculating them into the memory state with both inputs set low, the cells remained ON (steps 3 and 4). Notably, the cells at step 4 are at the same inducer concentrations as used at step 2, but the cells after step 4 are ON compared with being OFF after step 2. After 12 h in the memory state, we observed that <2% of the cells switched to the incorrect state. Finally, we could reset the latch by pulsing the cells with excess arabinose to force them OFF again (step 5).

Discussion

While bistability from sequestration has been shown *in vitro* (Kim et al, 2006), we have implemented a previously proposed design (Francois and Hakim, 2004) and verified *in vivo* that bistability can be generated without relying on cooperative transcription factors. Recent papers have suggested other methods for building bistability in the absence of cooperativity. Modeling of the MprA/MprB system in mycobacteria illustrated that sequestration of a sigma factor by its anti-sigma factor could have a critical role in allowing bistability in the natural system, and they propose experiments to demonstrate their predictions *in vivo* (Tiwari et al, 2010). Alternatively, nonlinearity in growth rate combined with positive feedback could result in bistability (Tan et al, 2009), but the *in vivo* synthetic system did not exhibit steady-state hysteresis on the population level, indicating that building memory units based on this design could be problematic. Just recently, two positive feedback loops without cooperativity or other sources of ultrasensitivity were theoretically shown to be sufficient to generate bistability (Palani and Sarkar, 2011). While this is an elegant topology as the requirements are minimal and the design facilitates tuning, the *in vivo* system contained basal ultrasensitivity in one of the feedback loops, so this design remains to be demonstrated using pathways without inherent ultrasensitivity.

Biological devices should be evaluated in terms of operating performance and scalability. The key operational feature of our design is that it allows predictable tuning of the switching
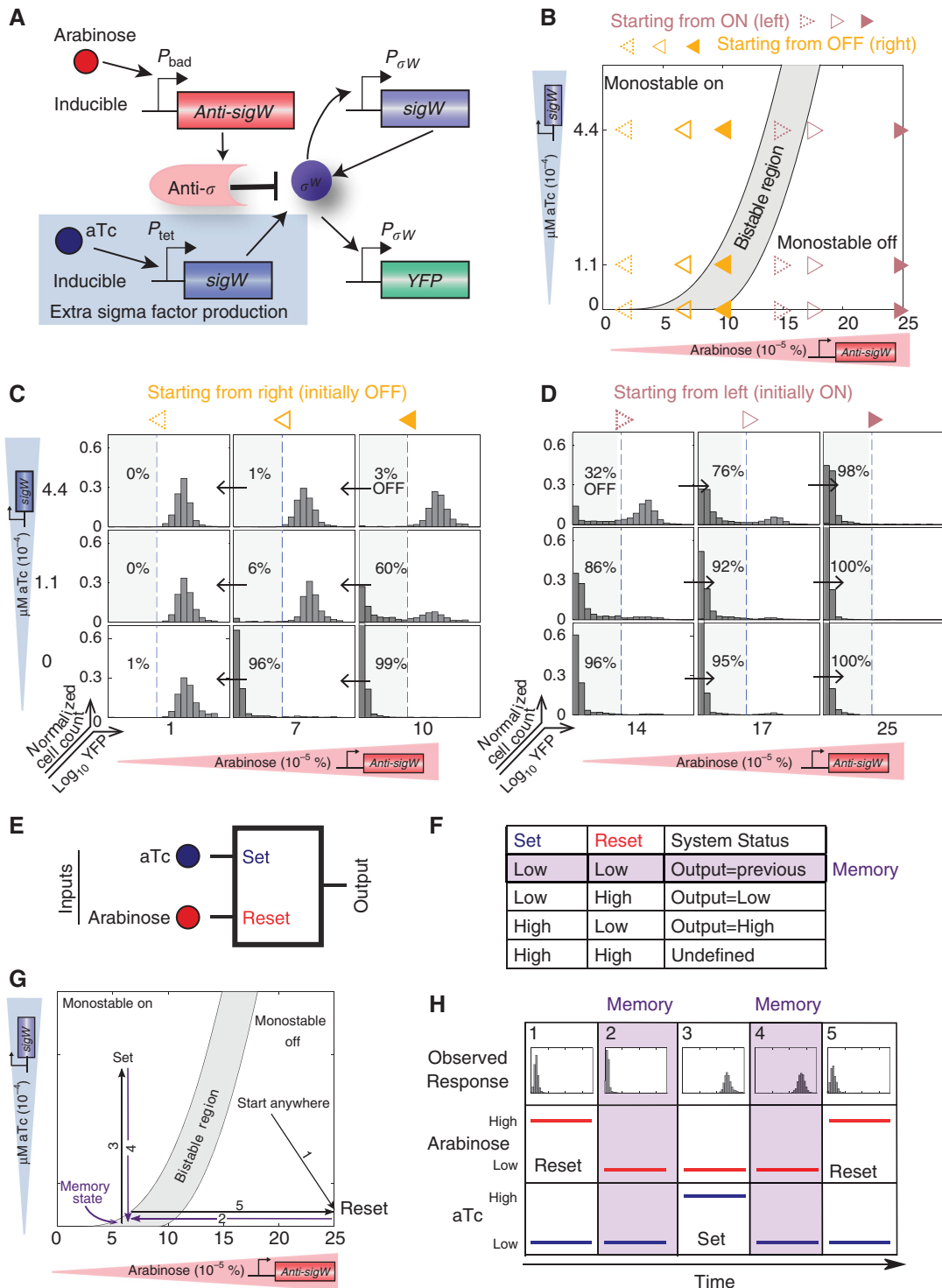
Figure 3 Sequestration-based bistability allows predictable tuning of the switching boundaries and design of a set–reset latch. (**A**) Schematic of system implemented in APA4310 cells with extra sigma factor production controlled by aTc induction (**B**) Bifurcation diagram overlaid with arrowheads denoting inducer concentrations where the system was investigated. Cells initially OFF were induced at the concentrations indicated with left arrowheads, and cells initially ON were induced at the concentrations marked with right arrowheads. (**C**) Histograms show that cells initially OFF switch ON at higher arabinose levels with increasing aTc induction. Cells were grown at the indicated arabinose and aTc concentrations (corresponding to left arrowheads from panel B) for 12 h, and at least 1000 cells were imaged per histogram. The percentage indicates the proportion of cells considered OFF (sum of bars in shaded area). (**D**) Cells initially ON require more arabinose to switch OFF with increasing aTc. Arabinose and aTc concentrations correspond to right arrowheads from panel B. (**E**) Schematic of set–reset latch. (**F**) Logic table corresponding to set–reset latch. (**G**) Using the previously determined switching boundaries, a set–reset latch can quickly be designed. Path numbers correspond to observed points in next panel. (**H**) The system retains a memory of the previous SET or RESET pulse. Steps 2 and 4 were analyzed after allowing the system to grow for 12 h, and cells were grown in the Set and Reset stages for 9 h. Source data is available for this figure in the Supplementary Information.

boundaries by adjusting expression of the sequestering protein. Another advantage is that the simple topology based on positive autoregulation lets us describe the key characteristics with analytical expressions (Supplementary information). Thus, if we desire a certain dynamic range or width of hysteretic region for a future application, the analytical results guide us in choosing optimal parameter values. One caveat with our system, however, is that the width of the hysteretic region is coupled with the tuning of the switching boundaries (Supplementary Figure 6 illustrates how the nullclines are shifted with increasing extra sigma factor production).

The scalability of any biological device is limited both by the number of orthogonal parts and by host interaction. We chose to use an extracytoplasmic function (ECF) sigma factor as the ECF sigma factors and non-ECF sigma factors recognize different consensus promoters via distinct mechanisms of promoter binding (Lane and Darst, 2006). There are 43 groups of ECF sigma factors that recognize different consensus promoters, and Ec contains two ECF sigma factors that belong to different groups than SigW's group (Staroń et al, 2009). As 35 of the ECF sigma factor groups have cognate anti-sigma factors that should be orthogonal, the strategy presented here should be scalable. We observe a small amount of crosstalk between SigW and SigE and their cognate promoters (Supplementary Figure 7), so using these systems in the same cell could require understanding the determinants of orthogonality. Host interaction could also be problematic as we see a mild effect on the growth rate when the sigma factor is expressed, but these could be resolved in the future by reducing the maximal rate of sigma factor production from the feedback loop or by identifying and fixing the parasitic interactions with the host.

Memory modules will be key components of synthetic biology applications in the future, so genetic engineers will need a large palette of different types to choose from. While the genetic toggle switch based on mutually inhibitory transcription factors has been the standard design for a set–reset latch (Gardner et al, 2000), each instance requires two cooperative transcription factors while our design requires only one activator/anti-activator pair per switch. Future work could further compare different properties of the competing designs; for example, the toggle switch was shown to be more robust to growth rate changes than a positive autoregulatory loop (Klumpp et al, 2009). An in vivo demonstration for a T-latch was also recently published, which features a push-on and push-off behavior (Lou et al, 2010).

Although we have focused on bistability, memory units can also be built on recombinases (Ham et al, 2008; Friedland et al, 2009), which may be especially attractive for long-term storage, but these devices lack a hysteretic region that provides buffering and the scalability of these parts is still unproven. A recent design based on recombinases especially demonstrated the stability of the device over 120 doublings, although switching was only 85% complete after a RESET pulse (Bonnet et al, 2012). In contrast, our device is 99% complete in switching after either a SET or RESET pulse of 9 h, but we find that the half-life of the ON state in the memory region is only 24 h. Our current device may not be suitable for applications that require long-term stability, but this could

be improved in the future; for example, if the mild growth defect was fixed and both states grew at the same rate, the half-life of the ON state should be about 43 h. The sequestration-based switch should be advantageous for applications requiring scalability and predictable tuning.

Materials and methods

Modeling

Bifurcation diagrams were computed from a simple model described in the Supporting information, using experimentally measured induction curves (shown in Supplementary Figures 9 and 10). The Supporting Information also provides an analytical treatment of the system, and the width of the hysteretic region as a function of the two key parameters is shown in Supplementary Figure 11.

Cloning details

The $sigW$ and $rsiW$ genes were cloned from B. subtilis 168 (Bs) genomic template using primers o330/o331 for $sigW$ and o332/o333 for $rsiW$ (oligonucleotide sequences are in Supplementary Table 3). When we express the anti-sigma factor $rsiW$ in Ec, we only use the N-terminal 87 amino acids as this domain normally remains in the cytoplasm, does not contain residues that target RsiW for proteolytic degradation, and was previously found to be sufficient to sequester the sigma factor in Bs (Schöbel et al, 2004; Zellmeier et al, 2006). For the SigW-dependent promoter, we cloned the promoter that drives the $sigW/rsiW$ operon in Bs (using primers o328/o329) (Qiu and Helmann, 2001). We observed some leakage from this promoter in the absence of $sigW$ expression, but this leakage was removed when we changed the UP element of the promoter to the Ec consensus (using oDC383/oDC384 and the Phusion Site-Directed Mutagenesis protocol). This modified promoter exhibits a 100-fold induction ratio and was used to control transcription of both the positive feedback loop and the YFP reporter.

As explained in the Supporting information, increasing maximal sigma factor production rate from the feedback loop (QUOTE in the model) increases the width of the hysteretic region and increases the difference between ON and OFF states. We selected for high expression by constructing an RBS library in the 5′-UTR region between PsigW and $sigW$ (using primers o362/o363) and screened for candidates that exhibited strong fluorescence when co-transformed with a reporter plasmid containing PsigW-GFP. We also created an RBS library for $rsiW$ expression (using primers o364/o365) and selected for an RBS that produced enough anti-sigma factor to turn off fluorescence from a strain containing PsigW-GFP and $sigW$ being expressed from the Ptet promoter.

The PsigW-sigW and Pbad-rsiW transcriptional units were placed on a high copy plasmid (pMB1 origin) with a strong transcriptional terminator (rrnB terminator) between them. The PsigW-Venus and Ptet-sigW transcriptional units were placed on a p15a plasmid, again with a strong transcriptional terminator between them. To facilitate debugging of the inducible promoters, RFP was added to the operon controlled by Pbad (using primers o404/o405 and o391/o406) and CFP was added to the operon controlled by Ptet (using o395/o396 and o390/o394) using SLIC (Li and Elledge, 2007). The Venus (YFP) and Cerulean (CFP) reporters were obtained from pZS2-123 (Cox et al, 2010). RFP is a codon-optimized mRFP obtained by Prof. J Christopher Anderson, UC Berkeley, from the Parts Registry (part E1010) and was modified at nucleotide positions 6–11 to fix an RBS issue.

The sigE switch based on R. sphaeroides was cloned using o416/o417 off pBS16 (Schilke and Donohue, 1995). The sigE/chrR system was previously shown to function in Ec (Newman et al, 2001). The reporter plasmid pDC311 was created by using o418/o419 off pDC288 to swap the sigW-responsive promoter with the sigE-responsive P1 promoter. Following the same procedure described above for the sigW-based switch, an RBS library was created between the P1-sigE 5′-UTR region using o420/o421 and the candidates were screened using pDC311. The chrR gene was also cloned from pBS16 using o422/o423 and used to replace $rsiW$ in pDC298 using SLIC with o424/o425. The

candidate from the RBS library (using o428/o429) and the Pbad-chrR (using o426/o427) operons were combined using SLIC to make pDC317.

Plasmid maps are provided in Supplementary Figure 8 for the SigW-based bistable system and Supplementary Table 2 contains the plasmids and strains. Plasmids were transformed into BW27783, a strain designed to allow homogeneous expression from the pBad promoter (Khlebnikov *et al*, 2001). Oligos were ordered from IDT with standard desalting.

Growth conditions

Cells were grown at 37°C in M9 minimal medium supplemented with glycerol and casamino acids; media contains per liter: 11.28 g 5 × M9 salt (Sigma M6030), 300 mg thiamine hydrochloride, 8 ml 50% glycerol, 2 g casamino acids (BD Bacto), 20 ml of 0.1 M magnesium sulfate, 200 μl of 0.5 M calcium chloride, filling to 1 l with distilled water, and filtering before storage at 4°C. Antibiotics were added as appropriate with carbenicillin at 50 μg/ml and chloramphenicol at 25 μg/ml. To prepare master cultures, cells were grown overnight in 0.1% arabinose (Sigma A3256) or the absence of arabinose to an OD600 of 0.1 and then stored in 10% glycerol aliquots of 50–100 μl at −80°C (8-strip PCR tubes, T-3135-1, from Bioexpress were found to be the most convenient for storing aliquots). Master cultures for Figure 3B–D were grown in the absence of aTc and 0 or 0.1% arabinose. The experiments were performed by thawing a frozen aliquot at 37°C for a minute and then diluting the cells 16-million-fold into 2 ml of the m9 medium. Cells were grown overnight at 37°C at 200 r.p.m. until an OD600 of ∼0.1 and then cells were concentrated via a microcentrifuge for microscopic analysis. For the tunable boundary experiments, cells were grown at the indicated concentrations of arabinose and aTc (Clontech 631310). For the set–reset latch experiments, cells were pulsed OFF by growing in 0.1% arabinose and in the absence of aTc. Cells were grown in the memory state in the absence of aTc and $6.3*10^{-5}$% arabinose. Cells were pulsed ON by growing at the same arabinose concentration and $\sim 10^{-3}$ μM aTc.

Microscopy

Cells were imaged on a Zeiss Axio Observer D1 using a 63 × plan-apochromat Ph3 oil-immersion objective. Cells were imaged with phase contrast and with the appropriate fluorescence filter set (38 for GFP/YFP, 45 for RFP, and 47 for CFP) with the following exposure times (150 ms for RFP, 50 ms for GFP/YFP, and 150 ms for CFP). Fluorescence excitation was provided with an X-CITE 120XL. Images were captured with an AxioCam MRm using the provided Zeiss Axiovision software.

Image analysis

Images were analyzed using Matlab software, starting with the routines provided with CellTracer (Wang *et al*, 2010). Phase contrast images were first thresholded and then segmented using the CTiterativeSelectiveSegmentation function, which recursively separates the cells in an area of the image. Cells were then discarded if they failed checks on eccentricity or size (removes clumps of cells that could not be segmented as individuals). Sample segmentation results are presented in Supporting Figure 12. After segmenting the phase contrast images, the fluorescence images were first flat-field normalized. Then the fluorescence for each cell in the image was calculated. For each cell, the background fluorescence in a 20-by-20 pixel box surrounding the cell was calculated and then subtracted from the mean fluorescence in the area within the cell. Finally, dead cells or debris misclassified as cells were removed by excluding cells that failed to exhibit any CFP when expected (i.e., cells containing pDC304 and grown in aTc induction or cells containing pDC297 with CFP under constitutive expression). For cells not expected to express CFP, cells were excluded if they failed to exhibit any RFP fluorescence. For most images, no more than 1% of the cells after segmentation were excluded as dead.

Other instruments

Bulk fluorescence measurements were performed on a Tecan Infinite M1000 (RFP settings were 584/607 nm for excitation and emission with 5 nm bandwidths, 0 μs lag, 20 μs integration, 50 reads, calculated z-position, and gain set to 170) or a Tecan Safire 2 (YFP measured with 510/528 excitation and emissions wavelengths and 5 nm bandwidths, 130 gain, 10 reads, and 20 μs integration). Optical density measurements were performed on an UVmini-1240 (Shimadzu).

Supplementary information

Supplementary information is available at the *Molecular Systems Biology* website (www.nature.com/msb).

Conflict of interest

The authors declare that they have no conflict of interest.

References

Acar M, Becskei A, van Oudenaarden A (2005) Enhancement of cellular memory by reducing stochastic transitions. *Nature* **435**: 228–232

Ajo-Franklin CM, Drubin DA, Eskin JA, Gee EPS, Landgraf D, Phillips I, Silver PA (2007) Rational design of memory in eukaryotic cells. *Genes Dev* **21**: 2271–2276

Angeli D, Ferrell JE, Sontag ED (2004) Detection of multistability, bifurcations, and hysteresis in a large class of biological positive-feedback systems. *Proc Natl Acad Sci USA* **101**: 1822–1827

Atkinson MR, Savageau MA, Myers JT, Ninfa AJ (2003) Development of genetic circuitry exhibiting toggle switch or oscillatory behavior in *Escherichia coli*. *Cell* **113**: 597–607

Bashor CJ, Helman NC, Yan S, Lim WA (2008) Using engineered scaffold interactions to reshape MAP kinase pathway signaling dynamics. *Science* **319**: 1539–1543

Becskei A, Seraphin B, Serrano L (2001) Positive feedback in eukaryotic gene networks: cell differentiation by graded to binary response conversion. *EMBO J* **20**: 2528–2535

Bonnet J, Subsoontorn P, Endy D (2012) Rewritable digital data storage in live cells via engineered control of recombination directionality. *PNAS* **109**: 8884–8889

Buchler NE, Cross FR (2009) Protein sequestration generates a flexible ultrasensitive response in a genetic network. *Mol Syst Biol* **5**: 272

Buchler NE, Louis M (2008) Molecular titration and ultrasensitivity in regulatory networks. *J Mol Biol* **384**: 1106–1119

Burrill DR, Silver PA (2010) Making cellular memories. *Cell* **140**: 13–18

Cox RS, Dunlop MJ, Elowitz MB (2010) A synthetic three-color scaffold for monitoring genetic regulation and noise. *J Biol Eng* **4**: 10

Ferrell JE (1996) Tripping the switch fantastic: how a protein kinase cascade can convert graded inputs into switch-like outputs. *Trends Biochem Sci* **21**: 460–466

Ferrell JE (2002) Self-perpetuating states in signal transduction: positive feedback, double-negative feedback and bistability. *Curr Opin Cell Biol* **14**: 140–148

Francois P, Hakim V (2004) Design of genetic networks with specified functions by evolution in silico. *Proc Natl Acad Sci USA* **101:** 580–585

Friedland AE, Lu TK, Wang X, Shi D, Church G, Collins JJ (2009) Synthetic gene networks that count. *Science* **324:** 1199–1202

Gardner TS, Cantor CR, Collins JJ (2000) Construction of a genetic toggle switch in *Escherichia coli*. *Nature* **403:** 339–342

Ham TS, Lee SK, Keasling JD, Arkin AP (2008) Design and construction of a double inversion recombination switch for heritable sequential genetic memory. *PLoS ONE* **3:** e2815

Khlebnikov A, Datsenko KA, Skaug T, Wanner BL, Keasling JD (2001) Homogeneous expression of the PBAD promoter in *Escherichia coli* by constitutive expression of the low-affinity high-capacity AraE transporter. *Microbiology* **147:** 3241–3247

Kim SY, Ferrell Jr JE (2007) Substrate competition as a source of ultrasensitivity in the inactivation of Wee1. *Cell* **128:** 1133–1145

Kim J, White KS, Winfree E (2006) Construction of an *in vitro* bistable circuit from synthetic transcriptional switches. *Mol Syst Biol* **2:** 68

Klumpp S, Zhang Z, Hwa T (2009) Growth rate-dependent global effects on gene expression in bacteria. *Cell* **139:** 1366–1375

Kramer BP, Fussenegger M (2005) Hysteresis in a synthetic mammalian gene network. *Proc Natl Acad Sci USA* **102:** 9517–9522

Lane WJ, Darst SA (2006) The structural basis for promoter −35 element recognition by the group IV σ factors. *PLoS Biol* **4:** e269

Lee T-H, Maheshri N (2012) A regulatory role for repeated decoy transcription factor binding sites in target gene expression. *Mol Syst Biol* **8:** 576

Li MZ, Elledge SJ (2007) Harnessing homologous recombination *in vitro* to generate recombinant DNA via SLIC. *Nat Meth* **4:** 251–256

Lou C, Liu X, Ni M, Huang Y, Huang Q, Huang L, Jiang L, Lu D, Wang M, Liu C, Chen D, Chen C, Chen X, Yang L, Ma H, Chen J, Ouyang Q (2010) Synthesizing a novel genetic sequential logic circuit: a push-on push-off switch. *Mol Syst Biol* **6:** 350

Lu MS, Mauser JF, Prehoda KE (2011) Ultrasensitive synthetic protein regulatory networks using mixed decoys. *ACS Synth Biol* **1:** 65–72

Nevozhay D, Adams RM, Van Itallie E, Bennett MR, Balázsi G (2012) Mapping the environmental fitness landscape of a synthetic gene circuit. *PLoS Comput Biol* **8:** e1002480

Newman JD, Anthony JR, Donohue TJ (2001) The importance of zinc-binding to the function of *Rhodobacter sphaeroides* ChrR as an anti-sigma factor. *J Mol Biol* **313:** 485–499

Ozbudak EM, Thattai M, Lim HN, Shraiman BI, van Oudenaarden A (2004) Multistability in the lactose utilization network of *Escherichia coli*. *Nature* **427:** 737–740

Palani S, Sarkar CA (2011) Synthetic conversion of a graded receptor signal into a tunable, reversible switch. *Mol Syst Biol* **7:** 480

Qiu J, Helmann JD (2001) The {-}10 region is a key promoter specificity determinant for the *Bacillus subtilis* extracytoplasmic-function {sigma} factors {sigma}X and {sigma}W. *J Bacteriol* **183:** 1921–1927

Ray JCJ, Tabor JJ, Igoshin OA (2011) Non-transcriptional regulatory processes shape transcriptional network dynamics. *Nat Rev Microbiol* **9:** 817–828

Schilke BA, Donohue TJ (1995) ChrR positively regulates transcription of the *Rhodobacter sphaeroides* cytochrome c2 gene. *J. Bacteriol* **177:** 1929–1937

Schöbel S, Zellmeier S, Schumann W, Wiegert T (2004) The *Bacillus subtilis*σW anti-sigma factor RsiW is degraded by intramembrane proteolysis through YluC. *Mol Microbiol* **52:** 1091–1105

Staroń A, Sofia HJ, Dietrich S, Ulrich LE, Liesegang H, Mascher T (2009) The third pillar of bacterial signal transduction: classification of the extracytoplasmic function (ECF) σ factor protein family. *Mol Microbiol* **74:** 557–581

Tan C, Marguet P, You L (2009) Emergent bistability by a growth-modulating positive feedback circuit. *Nat Chem Biol* **5:** 842–848

Tiwari A, Balázsi G, Gennaro ML, Igoshin OA (2010) The interplay of multiple feedback loops with post-translational kinetics results in bistability of mycobacterial stress response. *Phys Biol* **7:** 036005

Trunnell NB, Poon AC, Kim SY, Ferrell Jr JE (2011) Ultrasensitivity in the regulation of Cdc25C by Cdk1. *Mol Cell* **41:** 263–274

Wang Q, Niemi J, Tan C, You L, West M (2010) Image segmentation and dynamic lineage analysis in single-cell fluorescence microscopy. *Cytometry A* **77A:** 101–110

Zellmeier S, Schumann W, Wiegert T (2006) Involvement of Clp protease activity in modulating the *Bacillus subtilis*σW stress response. *Mol Microbiol* **61:** 1569–1582